

Article



Journal of Vibration and Control 2024, Vol. 30(5-6) 1286–1296
© The Author(s) 2023
Article reuse guidelines:
sagepub.com/journals-permissions
DOI: 10.1177/10775463231161389
journals.sagepub.com/home/jvc



Suppress chatter in milling of thin-walled parts via fixture with active support

Xingjian Dong , Guowei Tu , Lan Hu2, and Zhike Peng , and Zhike Peng ,

Abstract

In this study, we designed an integrated fixture system using eddy current sensors and piezoelectric actuators. With this system, active supporting forces are exerted on thin-walled workpieces to adjust their stiffness in a real-time manner and thus to suppress chatter in milling. When modeling this system, we used a mass-stiffness-damping element to characterize the dynamic behavior of the actuator under high-speed responses, and we considered the electromechanical coupling between the mechanical elements and the drive circuit of the actuator. We then proposed an optimal delayed state feedback controller for the closed-loop system. The delayed state is obtained by introducing the time delay in milling dynamics into the regular state feedback, and the optimal gain is worked out through the differential quadrature and gradient descent, which is a much more computationally efficient method than the classic semi-discretization. Among all similar approaches, our strategy leads to the largest stability region for milling of thin-walled parts and requires the least energy input, which are proved by simulations and experiments.

Keywords

Milling chatter, active control, thin-walled parts, piezoelectric actuators, delayed state feedback

I. Introduction

Chatter has always been an issue in milling, especially when it comes to thin-walled parts (Hao et al., 2022b), and one common strategy for chatter suppression is active control (Quintana and Ciurana, 2011; Zhu and Liu, 2020). Spindle speed variation (SSV) is a classic active control technique. When chatter occurs, the spindle speed continuously varies to interfere with the formation of chatter marks. Multiple patterns for such variation exist: sinusoidal (Yamato et al., 2018, 2020), triangular (Nam et al., 2020; Seguy et al., 2011), square (Al-Regib et al., 2003), and even stochastic (Yilmaz et al., 2002) and chaotic (Fansen et al., 2011). Chatter could be exacerbated with a wrong pattern (Seguy et al., 2010), and yet no general rules can be followed to choose the pattern (including the waveform, amplitude, and frequency). Besides, frequent speed changes cause damage to the spindle system. Therefore, the SSV has not been adopted extensively.

Another main strategy for active chatter control is the "smart spindle." For example, Monnin et al. (2014) mounted the accelerometer and piezoelectric stack on the front bearing of the spindle and thus developed a closed-loop system. Active radial control forces are exerted onto the spindle to suppress chatter. Modification of the spindle makes this strategy too costly and complicated to implement.

Unlike the above two solutions, auxiliary fixture/support is a strategy where the workpiece, instead of the spindle, is

controlled. Sensors and actuators are mounted on the fixture to enhance the stiffness and damping of the workpiece. This method is well suited for milling of thin-walled parts, where the flexible workpiece, rather than the spindle, is the main source of vibration. However, most studies only focus on quasi-static deformation control. Take the mirror milling system (MMS), a typical type of auxiliary support, for example. Sheng and Zhang (2018) used the MMS to maintain a constant supporting force on the thin-walled part, and Wang et al. (2019) adopted the MMS to achieve an iterative deformation compensation. Dynamic chatter control is not the focus of these studies. In this study, we designed an integrated fixture using eddy current sensors and piezoelectric actuators. Active dynamic supporting

¹State Key Laboratory of Mechanical System and Vibration, School of Mechanical Engineering, Shanghai Jiao Tong University, Shanghai, China ²Shanghai Aerospace Equipment Manufacturer Co. Ltd., Shanghai, China ³School of Mechanical Engineering, Ningxia University, Ningxia, China

Received: 12 July 2022; revised: 31 December 2022; accepted: 12 February 2023

Corresponding author:

Xingjian Dong, State Key Laboratory of Mechanical System and Vibration, School of Mechanical Engineering, Shanghai Jiao Tong University, Shanghai 200240, China.

Email: donxij@sjtu.edu.cn

forces are applied to the thin-walled workpiece to eliminate chatter. Extremely quick responses of eddy current sensors and piezoelectric actuators make our device especially suitable for highly dynamic chatter issues in engineering.

After we built the hardware, system modeling became a major task. Since the models of milling processes are well developed, the emphasis is on the actuator sub-system. Many researchers consider the relationship between the drive voltage and the output displacement/force of the actuator as linear (Sallese et al., 2017; Zhang et al., 2019), but this is incorrect when it comes to milling of thin-walled parts where a high spindle speed is adopted and thus a high response rate is set for the actuator (Georgiou and Mrad, 2005; Liu et al., 2013a). In that case, dynamic behavior of the actuator cannot be neglected. Therefore, in this study, we used the mass–stiffness–damping model to capture the dynamic behavior of the actuator and considered the coupling between the drive circuits and mechanical elements. Such an accurate dynamic model leads to better control performance.

Besides hardware building and system modeling, controller design is another major task. Chatter control is often viewed as vibration control for thin-walled parts under random disturbances (Zhang and Sims, 2005), that is, the time delay in milling dynamics is omitted, and thus, controllers typically for linear time invariant systems (such as PID) have been used for chatter suppression. However, the stability region of the milling system can be expanded much more efficiently if the time delay can be considered in controller design (Liu et al., 2013b, 2014; Long et al., 2017). In this study, we proposed an optimal delayed state feedback as the controller, where the time delay in milling dynamics is intentionally introduced into the state feedback and the optimal gain is calculated through the differential quadrature (DQ) method. Simulations and experiments demonstrate that our strategy helps to maximize the stability region of the thinwalled part milling system and requires minimal energy input.

2. System design and modeling

2.1. Design of fixture with active support

Figure 1 gives the fixture we designed, which is based on a regular vise. In this system, an eddy current sensor (measuring range = ± 1 mm) is used to measure the displacement of the workpiece, four piezoelectric actuators (drive voltage = 0–150 V, maximum output displacement = 152 μ m, and maximum output force = 1200 N¹) are used to exert active supporting forces on the workpiece, and four force sensors are used to measure the forces. A preload device is used to ensure constant contact between the workpiece and the actuator. Considering that the output force of the piezoelectric element is unidirectional, we installed the actuators on both sides. That is, when the control voltage is positive, we apply it to the actuators on

one side, otherwise we apply it to the actuators on the other side. More details about the fixture design are given in Section S1 in Supplementary Material.

2.2. Modeling of spindle—workpiece—actuator system

Next, we model the spindle–workpiece–actuator system in Figure 1. As we already modeled the same spindle–workpiece system without active support in our previous research work (Tu et al., 2021), the focus here is on the modeling of the actuator. Many researchers use a purely linear function to describe the relationship between the voltage applied to the piezoelectric actuator and the output displacement/force, but this only works if the response of the actuator is quasi-static. When milling thin-walled parts, we normally set the spindle speed very high and thus set the sampling frequency and the response rate of the actuator high. In this case, the dynamic behavior of the actuator cannot be neglected and the coupling between the actuator, workpiece, and milling tool must be considered. To this end, we establish an electromechanical model of the actuator and workpiece as a whole.

Figure 2 shows the model we built. The actuator subsystem consists of the drive circuit (including the capacitor c and resistor r) and mechanical elements (including the mass m_p , stiffness k_p , and damping c_p). The contact stiffness between the workpiece and the actuator is not considered, that is, the two are regarded as being rigidly connected in a parallel manner. Note that the single actuator that can deliver bidirectional forces in Figure 2 is equivalent to the pair of actuators that are symmetrically installed on both sides of the workpiece in Figure 1. When the external voltage v_{in} is applied, the piezoelectric element is driven by the voltage v_e , and the entire system is subject to the active control force $F_p(t)$ and the external load $-F_y(t)$ (i.e., the projection of the milling force along the y axis (Tu et al., 2021)). The governing equation of this workpiece—actuator system is formulated as

$$(m_{wy} + m_p) \ddot{y}_w + (c_{wy} + c_p) \dot{y}_w + (k_{wy} + k_p) y_w$$

= $-F_v(t) - F_p(t)$. (1)

 $F_p(t)$ in equation (1) is given by

$$F_p(t) = T_{em} v_e(t), \tag{2}$$

where T_{em} is the electromechanical coupling coefficient and $v_e(t)$ is controlled by (Liu et al., 2013a)

$$v_{in}(t) = rc\dot{v}_e(t) + v_e(t). \tag{3}$$

Equations (1)–(3) describe the mechanical part, electronic part, and coupling effect, respectively. We then substitute these equations into the developed spindle–workpiece model (Tu et al., 2021), and we obtain an explicit model of the entire spindle–workpiece–actuator system as

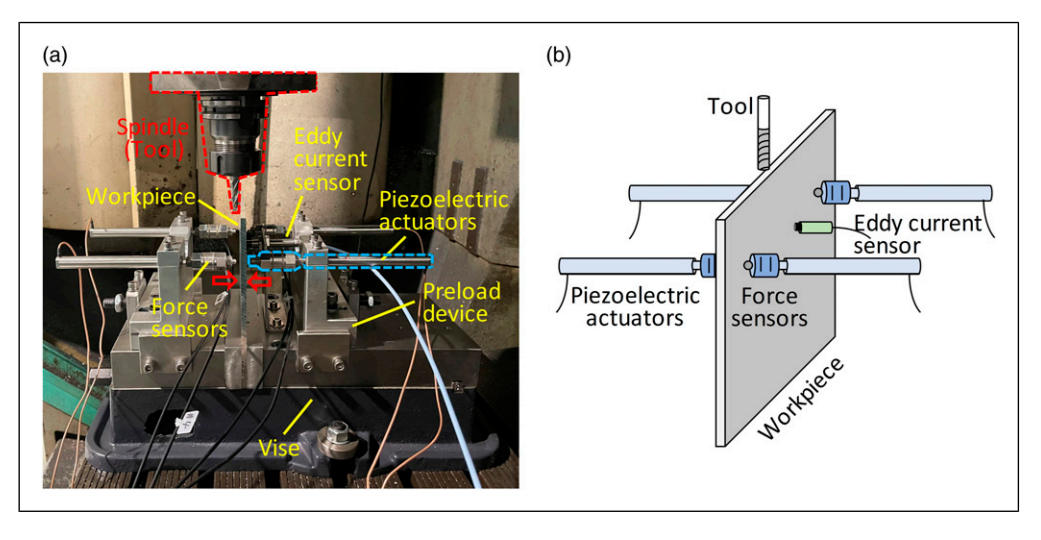


Figure 1. Designed fixture with active support: (a) picture and (b) sketch.

which is a six-dimensional, piecewise linear, periodically time-varying system with a constant time delay. The physical meanings and detailed expressions of all variables in equation (4) can be found in Section S2 in Supplementary Material. Next, we design the controller for this spindle—workpiece—actuator system.

3. Controller design: Optimal delayed state feedback

3.1. Delayed state feedback

Time delays have always been considered undesirable in controllers, but for dynamical systems that naturally have

inevitable time delays (such as the milling system discussed here), intentionally introduced time delays in controllers may have favorable effects in terms of the system stability (Liu et al., 2013b, 2014; Long et al., 2017). Following such an idea, we here design the delayed state feedback controller for the system equation (4).

As Figure 3 shows, the red rectangle denotes the controlled system and the blue rectangle denotes the state feedback, in which \mathbf{K}_1 is the feedback gain corresponding to the current state and \mathbf{K}_2 is the one corresponding to the delayed state. Considering that the reference input is zero (i.e., the ideal displacement is zero) and thus there will be no steady-state error in theory, we use the proportional-derivative (PD) controller. In this case, the observation matrix \mathbf{D} is given by

$$\mathbf{D} = \begin{pmatrix} 0 & 0 & 0 & 0 & 1 & 0 & 0 \\ 0 & 0 & 0 & 0 & 0 & 1 & 0 \end{pmatrix}, \tag{5}$$

and the system output is $\mathbf{y} = (y_w \ \dot{y}_w)^T$. The corresponding gain matrices are $\mathbf{K}_1 = (p_1 \ d_1)$ and $\mathbf{K}_2 = (p_2 \ d_2)$. We then can obtain the system input $v_{in}(t)$ as

$$v_{in}(t) = \mathbf{K}_1 \mathbf{y} + \mathbf{K}_2 \mathbf{y}(t - \tau). \tag{6}$$

Finally, the governing equation of the entire control loop in Figure 3 can be derived as

$$\dot{\tilde{\mathbf{x}}}(t) = (\tilde{\mathbf{A}} + \mathbf{C}\mathbf{K}_1\mathbf{D})\tilde{\mathbf{x}}(t) + (\tilde{\mathbf{B}} + \mathbf{C}\mathbf{K}_2\mathbf{D})\tilde{\mathbf{x}}(t - \tau).$$
 (7)

When proper gain parameters are set, the time delay $\tilde{\mathbf{x}}(t-\tau)$ in equation (7) may be eliminated and the stability region for the milling process may be maximized. Due to the time delay in the closed-loop system, it is difficult to use empirical rules to tune the delayed-PD controller (Dong et al., 2015). We here calculate the optimal gain based on the stability analysis of the control loop in Figure 3.

3.2. Optimal gain in the sense of stability

Improving the stability of the milling system is the fundamental strategy to suppress chatter, and therefore, we define the optimal gain in the sense of stability. We first rewrite equation (7) as

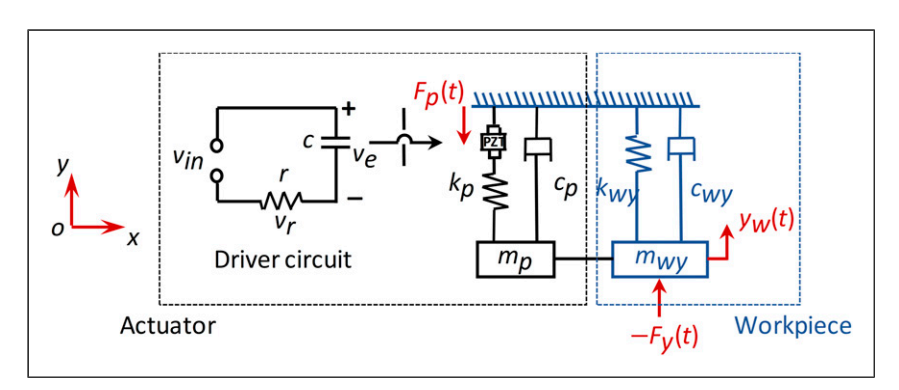


Figure 2. The electromechanical model of the workpiece-actuator system.

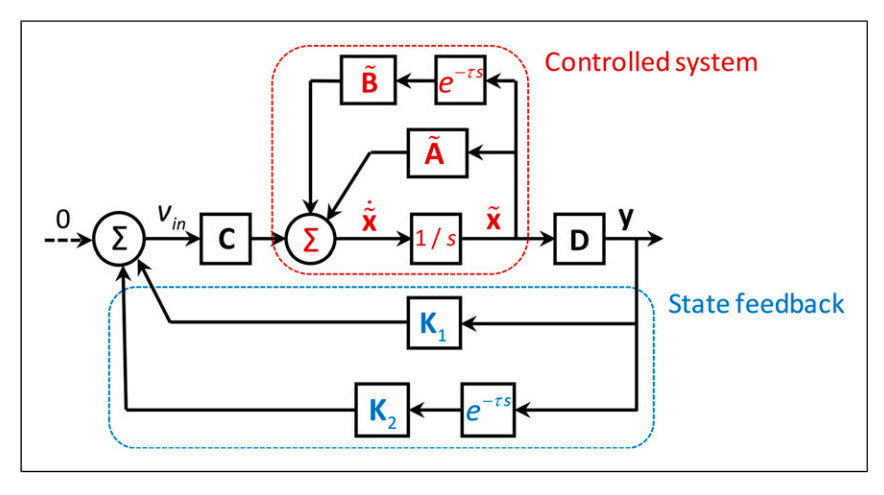


Figure 3. Block diagram of the closed-loop system, which consists of the controlled system (equation (4)) and the corresponding delayed state feedback controller.

$$\dot{\tilde{\mathbf{x}}}(t) = \tilde{\tilde{\mathbf{A}}}(t)\tilde{\mathbf{x}}(t) + \tilde{\tilde{\mathbf{B}}}(t)\tilde{\mathbf{x}}(t-\tau), \ \tilde{\tilde{\mathbf{A}}} = \tilde{\mathbf{A}} + \mathbf{C}\mathbf{K}_1\mathbf{D}, \tilde{\tilde{\mathbf{B}}} = \tilde{\mathbf{B}} + \mathbf{C}\mathbf{K}_2\mathbf{D},$$
(8)

where $\tilde{\mathbf{A}}$ and $\tilde{\mathbf{B}}$ are the new system matrices. Under the framework of the well-known semi-discretization method (Insperger and Stépán, 2004), the stability analysis of the system equation (8) boils down to the eigenvalue analysis of the state-transition matrix Φ . The matrix Φ can be regarded as a function of the gains \mathbf{K}_1 and \mathbf{K}_2 , and the criterion for a stable system is

$$\rho(\mathbf{\Phi}(\mathbf{K}_1, \mathbf{K}_2)) < 1, \tag{9}$$

where $\rho(\cdot)$ is an operator for the spectral radius of a matrix. When $\rho(\Phi(\mathbf{K}_1,\mathbf{K}_2))$ reaches its minimum, the milling response will decay fastest. Therefore, the optimal gain can be defined as

$$\mathbf{K}_{\text{opt}} = \underset{\mathbf{K}_1, \mathbf{K}_2 \in \Omega}{\operatorname{argmin}} \{ \rho(\mathbf{\Phi}(\mathbf{K}_1, \mathbf{K}_2)) \}, \tag{10}$$

where Ω is the region for optimal gain search.

We can of course solve the optimization problem equation (10) using the semi-discretization method. Once the gain parameters (K_1, K_2) have been specified, we can obtain the corresponding $\rho(\mathbf{\Phi})$ by the semidiscretization (Insperger and Stépán, 2004); and after iterating this process across the entire search region Ω , we can easily find the minimum of $\rho(\Phi)$ and the corresponding optimal gain. However, such a strategy is too computationally costly. One way to speed up this searching process is to obtain the partial derivatives of $\rho(\mathbf{\Phi})$ with respect to $(\mathbf{K}_1, \mathbf{K}_2)$ and then to use a generic optimizer such as the gradient descent. The partial derivatives cannot be obtained by a purely numerical method such as the semi-discretization. Here, we use a technique called the differential quadrature (DQ) (Bellman and Casti, 1971; Ding et al., 2013) to work out the analytical form of the matrix Φ with respect to the variables $(\mathbf{K}_1, \mathbf{K}_2)$, and thus to obtain the analytical form of the partial derivatives of $\rho(\Phi)$ with respect to $(\mathbf{K}_1, \mathbf{K}_2).$

Similar to the finite difference or finite element, the DQ is a method to numerically solve ordinary/partial differential equations. In the DQ, the derivative/partial derivative is approximated by a weighted sum of values of the integrand at specific grid points (Bellman and Casti, 1971). Before applying the DQ to equation (8), in order to simplify the computation, we neglect the nonlinearity in equation (8) (i.e., we omit the "loss-of-contact" effect in milling of thin-walled parts (Tu et al., 2021)), and we convert the periodically time-varying elements h(t) in the system matrices $\tilde{\bf A}$ and $\tilde{\bf B}$ in equation (8) to constants using the zero-order approximation (Gradišek et al., 2005) as

$$\overline{h} = \frac{1}{\tau} \int_0^{\tau} h(t) dt. \tag{11}$$

Then, we obtain the approximated closed-loop system as

$$\dot{\tilde{\mathbf{x}}}(t) = \overline{\mathbf{A}}\tilde{\mathbf{x}}(t) + \overline{\mathbf{B}}\tilde{\mathbf{x}}(t-\tau). \tag{12}$$

Under the framework of the DQ, the state-transition matrix of the system equation (12) is given by

$$\Phi = \Psi^{-1}\Gamma,$$

$$\Psi = -\begin{pmatrix} \mathbf{0}_{N\times N} & & \\ & \mathbf{I}_{n\times n} \otimes \overline{\mathbf{A}} \end{pmatrix} + \begin{pmatrix} \overline{\mathbf{I}}_{N\times N} | \mathbf{0}_{N\times Nn} \\ \frac{1}{\tau} \mathbf{D} \otimes \overline{\mathbf{I}}_{N\times N} \end{pmatrix},$$

$$\Gamma = \begin{pmatrix} \mathbf{0}_{N\times N} & \mathbf{0}_{N\times N} & \cdots & \mathbf{0}_{N\times N} & \mathbf{I}_{N\times N} \\ \mathbf{0}_{N\times N} & \overline{\mathbf{B}} & & \\ & \mathbf{0}_{N\times N} & \overline{\mathbf{B}} & & \\ \vdots & & \ddots & \\ & \mathbf{0}_{N\times N} & & \overline{\mathbf{B}} \end{pmatrix},$$

$$\vdots & & \ddots & \\ \mathbf{0}_{N\times N} & & \overline{\mathbf{B}} & & \\
\vdots & & \ddots & \\ & \overline{\mathbf{B}} & & \\
\vdots & & \ddots & \\
\mathbf{0}_{N\times N} & & \overline{\mathbf{B}} & & \\
\vdots & & \ddots & \\
\mathbf{0}_{N\times N} & & \overline{\mathbf{B}} & & \\
\vdots & & \ddots & \\
\mathbf{0}_{N\times N} & & \overline{\mathbf{B}} & & \\
\vdots & & \ddots & \\
\mathbf{0}_{N\times N} & & \overline{\mathbf{B}} & & \\
\vdots & & \ddots & \\
\mathbf{0}_{N\times N} & & \overline{\mathbf{B}} & & \\
\vdots & & \ddots & \\
\mathbf{0}_{N\times N} & & \overline{\mathbf{B}} & & \\
\vdots & & \ddots & \\
\mathbf{0}_{N\times N} & & \overline{\mathbf{B}} & & \\
\vdots & & \ddots & \\
\mathbf{0}_{N\times N} & & \overline{\mathbf{B}} & & \\
\vdots & & \ddots & \\
\mathbf{0}_{N\times N} & & \overline{\mathbf{B}} & & \\
\vdots & & \ddots & \\
\mathbf{0}_{N\times N} & & \overline{\mathbf{B}} & & \\
\vdots & & \ddots & \\
\mathbf{0}_{N\times N} & & \overline{\mathbf{B}} & & \\
\vdots & & \ddots & \\
\mathbf{0}_{N\times N} & & \overline{\mathbf{B}} & & \\
\end{bmatrix},$$

where N is the dimension of the closed-loop system equation (12), n is the number of grid points, and \mathbf{D} is a weight matrix. The derivation of equation (13) and the determination of the matrix \mathbf{D} are detailed in Section S3 in Supplementary Material.

In MATLAB programming, we first input the system matrices $\overline{\bf A}$ and $\overline{\bf B}$ and define the gain parameters $({\bf K}_1,{\bf K}_2)$ as symbolic variables. Then, we construct the matrices ${\bf \Psi}$ and ${\bf \Gamma}$ according to equation (13). We finally obtain the ${\bf \Psi}^{-1}$ using the MATLAB function inv and thus obtain the symbolic state-transition matrix ${\bf \Phi}({\bf K}_1,{\bf K}_2)$. Following this, we work out all the eigenvalues of the matrix ${\bf \Phi}$ (which are denoted by $\lambda({\bf \Phi})$) using the function eig, and we find out the one with the largest modulus (which is denoted by λ_ρ) after substituting the current gain parameters. With the eigenvalue λ_ρ , we calculate the partial derivative of the spectral radius of the state-transition matrix $\rho({\bf \Phi})$ with respect to the gain parameter z (z could be any of the parameters p_1, d_1, p_2, d_2) as

$$\frac{\partial \rho(\mathbf{\Phi})}{\partial z} = \frac{\partial \left| \lambda_{\rho} \right|}{\partial z} = \frac{\lambda_{\rho} \frac{\partial \overline{\lambda}_{\rho}}{\partial z} + \overline{\lambda}_{\rho} \frac{\partial \lambda_{\rho}}{\partial z}}{2 \left| \lambda_{\rho} \right|},\tag{14}$$

where $\bar{\lambda}_{\rho}$ is the conjugate of λ_{ρ} (see Section S4 in Supplementary Material for the derivation of equation (14)).

When using the DQ, we compute the state-transition matrix Φ only once before the searching process, and then we calculate the gradient $\partial \rho(\Phi)/\partial z$ at the current gain each time we update the gain. Due to its high computational efficiency, the gradient descent can lead to a much faster searching than that when the semi-discretization is used. We next demonstrate this point using a numerical case.

3.3. A numerical case

We consider a milling system that was numerically studied by Davies and Balachandran (2000). The number of tool teeth is set as 1, and the diameter of the tool is 8 mm; the specific cutting energy κ_t is 644 MPa, and the proportional factor κ_n is 0.37; the tool immersion ratio (i.e., a_e/D) is set as 0.05, and the feed rate is 0.01 mm/tooth. The structural parameters are given in Table 1. We set the spindle speed as $\Omega=17\times10^3$ rpm and the axial depth of cut as $a_p=2.5$ mm, in which case the milling system is going through quasi-periodic chatter (Tu et al., 2021). As for the actuator sub-system, we set the parameters as $m_p=9\times10^{-2}$ kg, $k_p=8\times10^6$ N/m, $c_p=50.89$ N/m s⁻¹, $c=2.4\times10^{-6}$ F, r=470 k Ω , and $T_{em}=3.67$ N/V (these parameters are obtained by system identification, which will be detailed in Section 5.2).

We here adopt the regular PD controller, that is, we make p_1 and d_1 the variables to be optimized while $p_2 = d_2 = 0$. The search region is set as $p_1 \in [-5, -40]$ and $d_1 \in [-10, 10]$. We first iterate the semi-discretization across the entire region so that we obtain the three-dimensional distribution of the spectral radius $\rho(\Phi)$ and find the optimal gain (which corresponds to the minimum of $\rho(\Phi)$), as shown in Figure 4(a). Then we use the DQ with gradient descent to do the searching. For the DQ, we set the number of grid points n as 40; and for the gradient descent, we set the initial value and the step size as $[p_1, d_1] = [-5, 0]$ and 0.5, respectively. Figure 4(b) shows the process of the gradient descent.

The optimal gain obtained by the semi-discretization is $(p_1, d_1)_{\text{opt}} = (-21.63, -1.40)$ (the blue " Δ " in Figure 4(b)),

corresponding to the $\min \rho(\Phi) = 0.76$; while the optimal gain obtained by the DQ with gradient descent is $(p_1,d_1)_{\rm opt} = (-21.62,-1.25)$ (the red "+" in Figure 4(b)), corresponding to the $\min \rho(\Phi) = 0.79$. The two methods lead to almost the same results, but the computational costs of these two strategies are hugely different. The searching by the semi-discretization takes 310 s; while through the DQ with gradient descent, the updated value converges to the minimum after only three iterations, taking 1.02 s. Our computationally efficient strategy is well suited for milling of thin-walled parts during which the system parameters may vary. We next apply the optimal delayed state feedback controller to the spindle—workpiece—actuator system, with the aim to demonstrate the effectiveness of the active support and the superiority of the controller we designed.

4. Control system simulation

As discussed in Section 3.2, the essence of chatter control is the expansion of the stability region. We here use control system simulation to show how the active support under delayed state feedback influences the stability region of the milling system for thin-walled parts. The parameters for simulation are the same as those used in Section 3.3. The stability lobe diagrams with different controllers used are given in Figure 5. Compared with the regular state feedback, the delayed state feedback helps to expand the stability region much more efficiently. When the delayed-PD controller is

Table 1. Structural parameters of the milling system for simulation (Davies and Balachandran, 2000).

	Mass (kg)	Stiffness (N m^{-1})	Damping (N s m^{-1})
Tool (x)	2.01 × 10 ⁻²	4.14 × 10 ⁵	1.56
Tool (y)	1.99×10^{-2}	4.09×10^5	1.60
Workpiece (y)	56.75	7.15 × 10 ⁶	1.68 × 10 ³

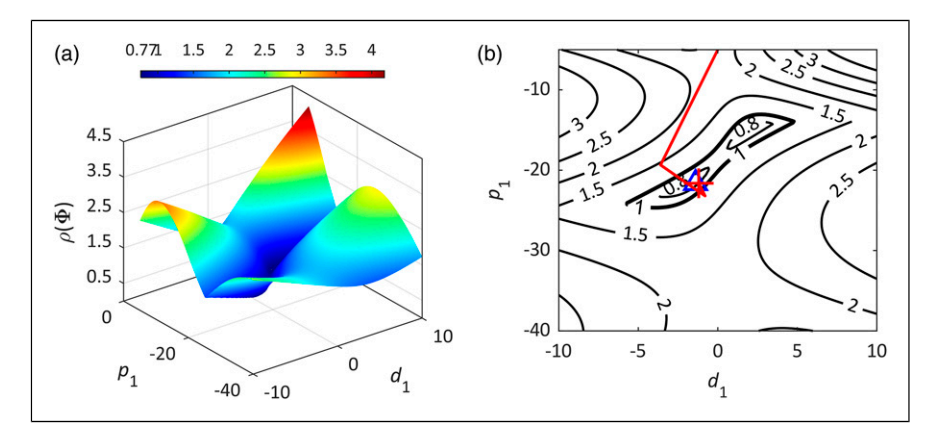


Figure 4. Searching for the optimal gain: (a) three-dimensional distribution of the spectral radius $\rho(\Phi)$ obtained by semi-discretization and (b) gradient descent with the aid of DQ.

adopted, the stability region is maximized, the area of which is about three times that of the uncontrolled milling system. In this case, the chatter instability can be well mitigated. We next verify the conclusion using experiments.

5. Experimental verification

5.1. Set-ub

The overall experimental set-up and the control logic flow are shown in Figure 6. We use an NI USB-6259 multifunctional I/O device to achieve the acquisition of the vibration signal and the output of the control signal. The calculation of the control signal is carried out by a LabVIEW program. All milling tests are conducted based on a DMU 70V five-axis vertical milling machine with the maximum spindle speed equal to 10,000 rpm. The aluminum thin-walled workpiece is clamped at one end, and the size of the free end is $100 \times 100 \times 3$ mm. The high-speed-steel milling tool is a single-tooth cutter with the diameter equal to 10 mm.

5.2. System identification

We next identify the milling system to obtain all the system parameters in equation (4). As Figure 7 shows, we first conducted modal tests on the milling tool, workpiece, and piezoelectric actuator to acquire the frequency responses (FRs) of these structures. We then obtained the structural parameters by fitting the experimental FRs, as given in Table 2. The electronic parameters of the actuator system are given in the product manual as $c = 2.4 \times 10^{-6}$ F and $r = 470 \Omega$. Next, we carried out the static loading test on the actuator (Georgiou and Mrad, 2005) to identify the electromechanical coupling coefficient as $T_{em} = 3.67 \text{ N/V}$. Last, using the algorithm proposed by Gradišek et al. (2004), we conducted some milling tests and identified the cutting force coefficients as $\kappa_t = 767.85$ MPa and $\kappa_n = 0.28$. With these parameters, the optimal gain can be calculated based on the strategy in Section 3.2.

5.3. Milling tests

We conducted milling tests to prove the effectiveness of the active support and the superiority of the controller we

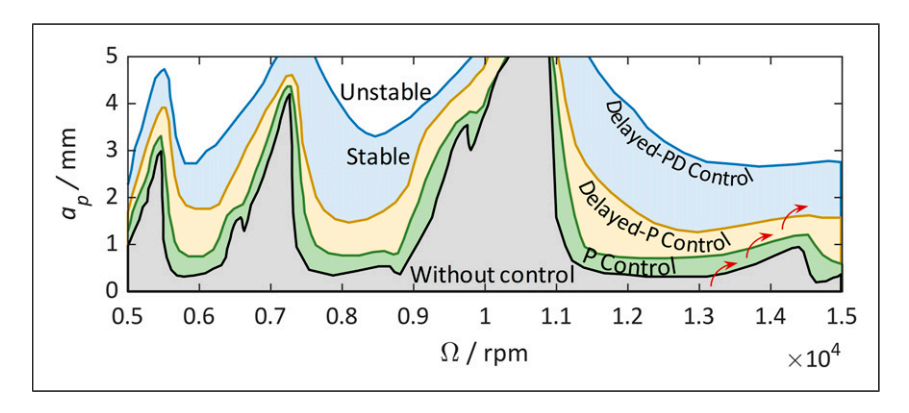


Figure 5. Stability lobe diagrams with different controllers used (all controller gains are obtained through the strategy in Section 3.2).

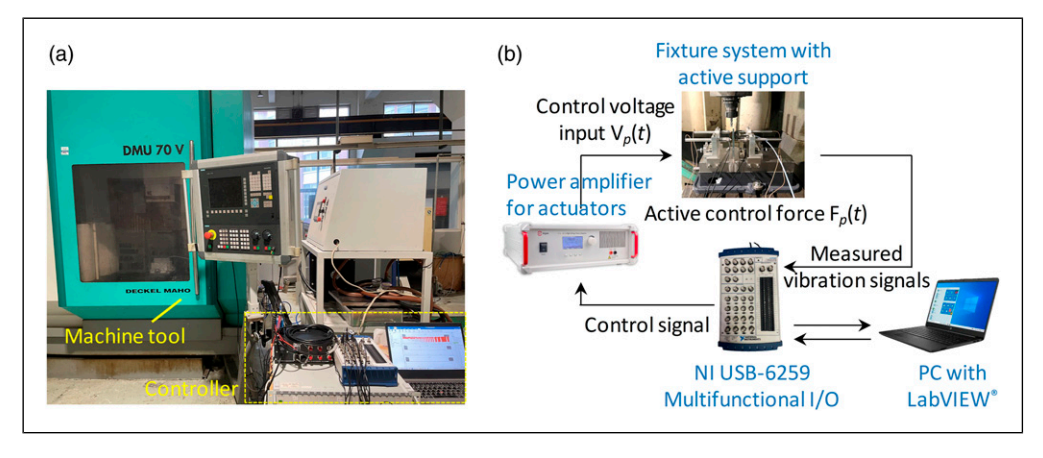


Figure 6. Experimental set-up: (a) overall view and (b) control logic flow.

designed. The sampling frequency was set as 10 kHz. Five controlled experiments (#1 ~ #5) were carried out: #1—without support (see Figure 8(a)), #2—support with control off (i.e., passive support, see Figure 8(b)), #3—support with delayed-PD feedback and optimal gain, #4—support with regular PD feedback and optimal gain, and #5—support with delayed-PD feedback and empirical gain. We used an online chatter prediction system that is based on our previous research work (Dong et al., 2021; Huangfu et al., 2022; Tu et al., 2020, 2021) (see Section S5 in Supplementary Material for details), and therefore, in the latter three tests (#3, #4, and #5), the controller automatically

turned on after the chatter alarm went off (Hao et al., 2022a; Liu et al., 2018; Zhao et al., 2021).

The same machining parameters were adopted in the above five tests: the spindle speed is 8000 rpm, and the feed rate is 0.0125 mm/tooth; the tool path is symmetrical about the midpoint of the free end of the workpiece with the length equal to 90 mm; the axial depth of cut increases from 1 mm to 10 mm at a constant rate, and the radial depth of cut remains constantly at 0.2 mm. Figure 9 gives the five sets of results, which include the surfaces of the workpiece, the collected displacement signals of the workpiece with a chatter indicator named the $H(\mathbf{s})$ (see Section S5 in

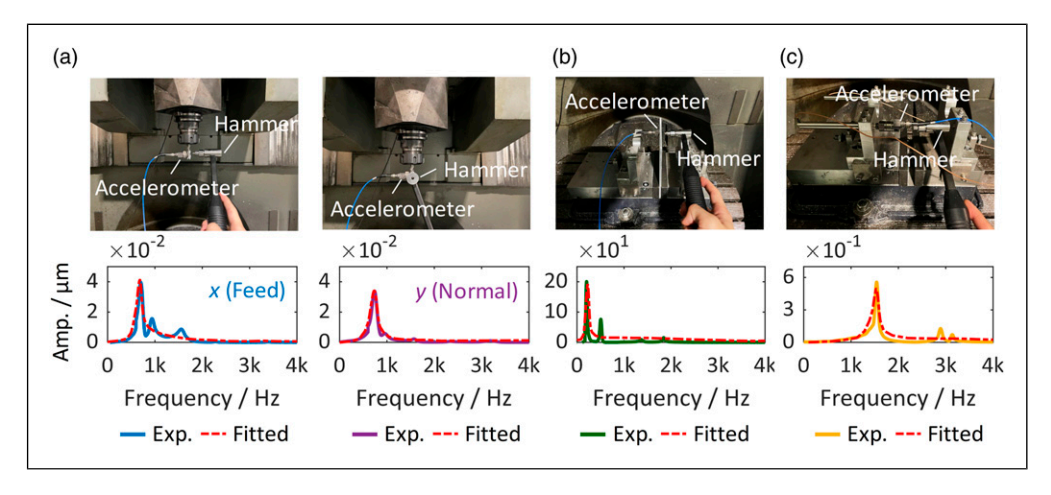


Figure 7. Modal tests and frequency responses of each component in the actively controlled milling system: (a) milling tool, (b) thin-walled workpiece, and (c) piezoelectric actuator.

Table 2. Structural parameters obtained by modal tests.

	Mass (kg)	Damping (Nem-1)	
	riass (kg)	Stiffness (Nm ⁻¹)	Damping (Nsm ⁻¹)
Tool (x)	6.7×10^{-2}	1.30 × 10 ⁶	13.15
Tool (y)	6.5×10^{-2}	1.29 × 10 ⁶	13.92
Workpiece (y)	2.1×10^{-1}	3.60×10^{5}	12.95
Actuator	9.0×10^{-2}	8.00 × 10 ⁶	50.89

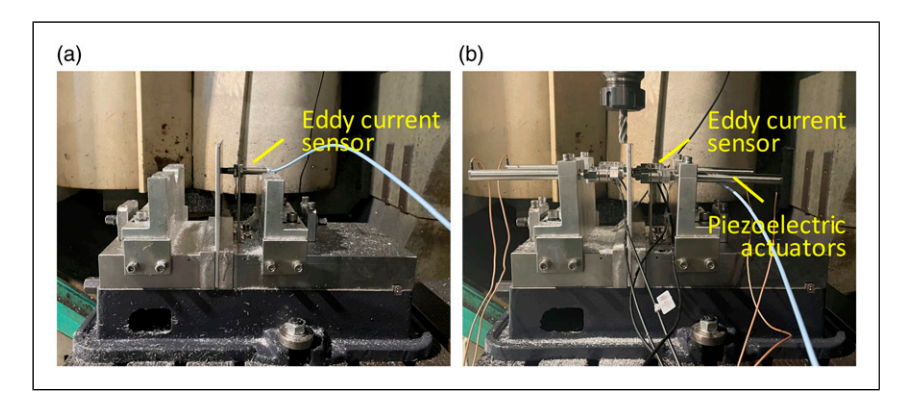


Figure 8. Fixture with and without support: (a) without support and (b) with support.

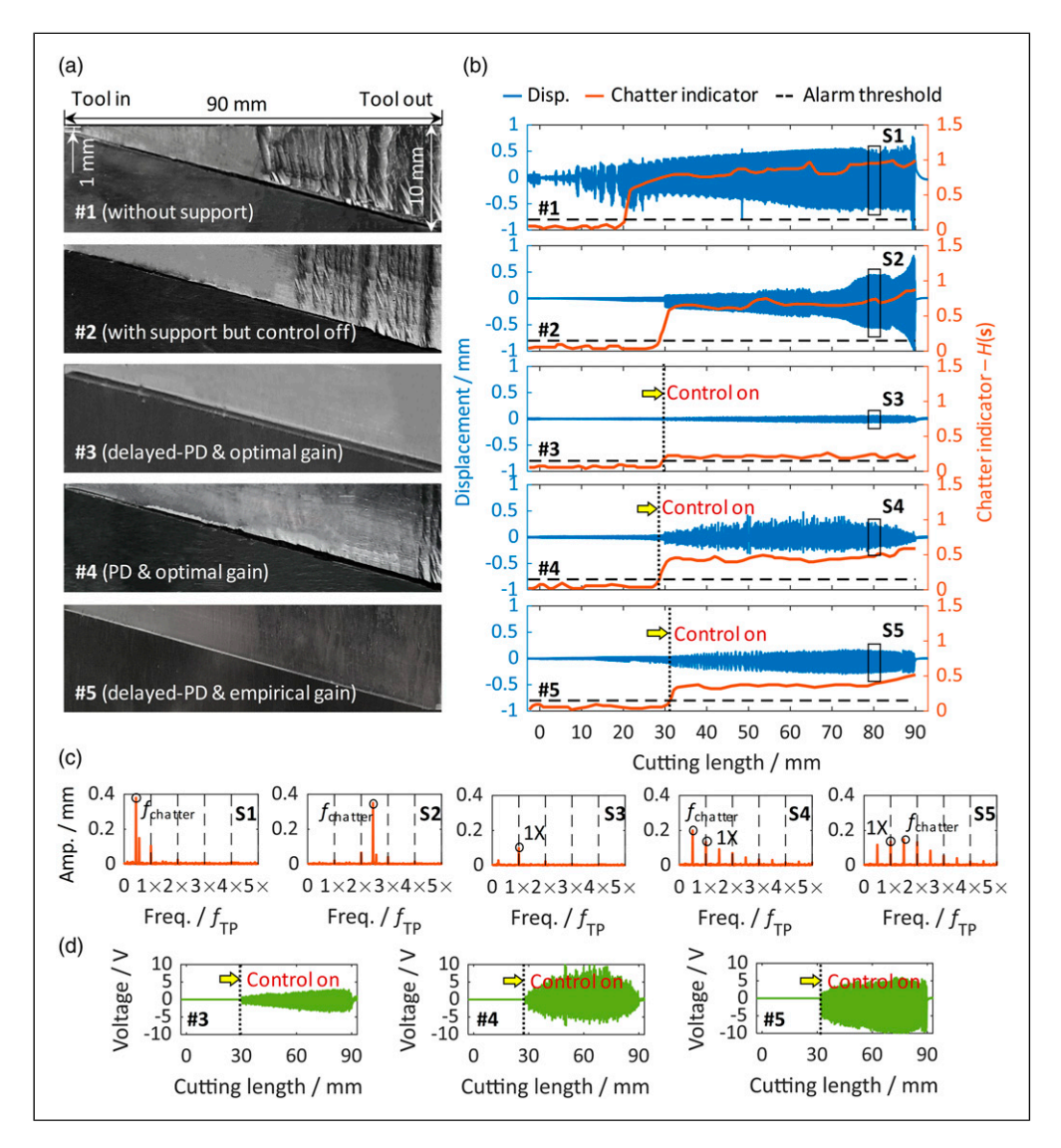


Figure 9. Five sets of results. (a) Surfaces of the workpiece. (b) Displacement responses of the workpiece with the chatter indicator (in tests #3, #4, and #5, the controllers were automatically turned on after the chatter alarm was triggered). (c) Fourier spectra of fives signal segments (SI \sim S5, as denoted in (b)). (d) Control voltages of the actuator in tests #3, #4, and #5.

Table 3. Standard deviation of the displacement signals.

Test number	#I (without support)	#2 (with support but control off)	#3 (delayed-PD and optimal gain)	#4 (PD and optimal gain)	#5 (delayed-PD and empirical gain)
Standard deviation	0.1978	0.1261	0.0133	0.0344	0.0654

Supplementary Material for how we calculate the H(s)), the Fourier spectra of the displacement signal segments, and the control voltages of the actuator.

Without support, the milling system went through severe chatter instability. As the axial depth of cut increased, the surface of the workpiece was damaged (see Figure 9(a) #1), the amplitude of vibration diverged (see Figure 9(b) #1), and the chatter frequency dominated the Fourier spectrum (see Figure 9(c) S1). Chatter was mitigated after the passive support was applied, but the similar instability-related

phenomena were still observed after a certain depth of cut was reached (see Figure 9(a) and (b) #2 and Figure 9(c) S2).

The optimal delayed-PD controller helped to eliminate chatter. As Figure 9(a) and (b) #3 shows, the displacement of the workpiece was within a small range, and the surface showed no chatter marks. In this case, the toothpassing frequency 1X instead of the chatter frequency dominated the Fourier spectrum (see Figure 9(c) S3). For comparison, we replaced the delayed-PD controller and the optimal gain with the regular PD controller and the empirical gain, respectively, in tests #3 and #4. This decreased the performance of the active support: chatter marks re-appeared (see Figure 9(a) #4 and #5), the amplitude increased (Figure 9(b) #4 and #5), and chatter components arose in the frequency domain (see Figure 9(c) S4 and S5). On top of that, the replacement intensified the energy consumption of the actuators, as Figure 9(c) shows. The results demonstrate the superiority of the active support under optimal delayed state feedback and the necessity of introducing such a strategy.

We also made a quantitative comparison in Table 3. We calculated the standard deviation (SD) of the displacement signals. With the controller turned off, the SD is large with or without support, which indicates severe chatter vibrations. While using active support combined with the optimal delayed-PD controller, we achieved stable milling with a much smaller SD. With the delayed-PD controller replaced by the regular PD controller or the optimal gain replaced by the empirical gain, the SD bounced back, which means the re-emergence of chatter. Please note that the chatter index H(s) shown in Figure 9(b) is also a quantitative indicator. The H(s) is derived from the time-frequency information of milling response signals (see Section S5 in Supplementary Material for details), and a higher H(s)value means more severe chatter. All these quantitative results have validated the qualitative analysis above.

6. Conclusions

In this study, we developed an active support system for thin-walled workpieces by integrating eddy current sensors and piezoelectric actuators into a fixture. With this system, the stiffness of the workpiece is adjusted in a real-time manner to suppress chatter. Some noteworthy conclusions are summarized as follows:

- (1) Under high-speed responses, the dynamic behavior of the piezoelectric actuator should be modeled for better chatter suppression performance. The mechanical part of the actuator can be described by a mass-stiffnessdamping element, and the electromechanical coupling between the mechanical part and the drive circuit (i.e., the electronic part) should be considered.
- (2) For milling systems where the time delay is naturally embedded, the delayed state can be intentionally

introduced into the regular state feedback to maximize the stability region and also minimize the energy input. To avoid empirical gain tuning, the differential quadrature combined with gradient descent can be utilized to work out the optimal gain in the sense of stability. This technique is much more computationally efficient than the classic semi-discretization.

In our experiments, the position of active support barely poses any influences on the performance of chatter suppression as the size of the thin-walled plate is quite small, but this is not true for relatively large thin-walled parts. In that case, we can build distributed support with each "small region" supported by a specific number of actuators. With such a strategy, the method we proposed can still be used. Our future work will be devoted to this.

Declaration of conflicting interests

The authors declared no potential conflicts of interest with respect to the research, authorship, and/or publication of this article.

Funding

The authors disclosed receipt of the following financial support for the research, authorship, and publication of this article: The research is supported by the National Natural Science Foundation of China [grant number 11872243] and the National Science and Technology Major Project of the Ministry of Science and Technology of China [grant number 2019ZX04025001].

ORCID iDs

Xingjian Dong https://orcid.org/0000-0003-1246-7604 Guowei Tu https://orcid.org/0000-0002-5178-2060 Zhike Peng https://orcid.org/0000-0002-2095-7075

Supplemental Material

Supplemental material for this article is available online.

Note

 The maximum output displacement and the maximum output force are both cited from the product manual of the piezoelectric actuators. The maximum output displacement is measured with zero load and maximum voltage applied, while the maximum output force is measured with zero displacement and maximum voltage applied.

References

Al-Regib E, Ni J and Lee S-H (2003) Programming spindle speed variation for machine tool chatter suppression. *International Journal of Machine Tools and Manufacture* 43(12): 1229–1240.
 Bellman R and Casti J (1971) Differential quadrature and long-term integration. *Journal of Mathematical Analysis and Applications* 34(2): 235–238.

- Davies MA and Balachandran B (2000) Impact dynamics in milling of thin-walled structures. Nonlinear Dynamics 22(4): 375–392.
- Ding Y, Zhu L, Zhang X, et al. (2013) Stability analysis of milling via the differential quadrature method. *Journal of Manufacturing Science and Engineering* 135(4): 044502.
- Dong W, Ding Y, Zhu X, et al. (2015) Optimal proportional—integral—derivative control of time-delay systems using the differential quadrature method. *Journal of Dynamic Systems*, *Measurement, and Control* 137(10): 101005.
- Dong X, Tu G, Wang X, et al. (2021) Real-time chatter detection via iterative Vold-Kalman filter and energy entropy. The International Journal of Advanced Manufacturing Technology 116(5): 2003–2019.
- Fansen K, Peng L and Xingang Z (2011) Simulation and experimental research on chatter suppression using chaotic spindle speed variation. *Journal of Manufacturing Science and Engineering* 133(1): 014502.
- Georgiou HMS and Mrad RB (2005) Electromechanical modeling of piezoceramic actuators for dynamic loading applications. *Journal of Dynamic Systems, Measurement, and Control* 128(3): 558–567.
- Gradišek J, Kalveram M, Insperger T, et al. (2005) On stability prediction for milling. *International Journal of Machine Tools* and Manufacture 45(7): 769–781.
- Gradišek J, Kalveram M and Weinert K (2004) Mechanistic identification of specific force coefficients for a general end mill. *International Journal of Machine Tools and Manufacture* 44(4): 401–414.
- Hao Y, Zhu L, Yan B, et al. (2022a) Milling chatter detection with WPD and power entropy for Ti-6Al-4V thin-walled parts based on multi-source signals fusion. *Mechanical Systems and Signal Processing* 177: 109225.
- Hao Y, Zhu L, Yan B, et al. (2022b) Stiffness design and multiobjective optimization of machine tool structure based on biological inspiration. *Journal of Vibration and Control*. DOI: 10.1177/10775463221085858
- Huangfu Y, Dong X, Chen K, et al. (2022) A tribo-dynamic based pitting evolution model of planetary gear sets: a topographical updating approach. *International Journal of Mechanical Sci*ences 220: 107157.
- Insperger T and Stépán G (2004) Updated semi-discretization method for periodic delay-differential equations with discrete delay. *International Journal for Numerical Methods in Engineering* 61(1): 117–141.
- Liu C, Zhu L and Ni C (2018) Chatter detection in milling process based on VMD and energy entropy. *Mechanical Systems and Signal Processing* 105: 169–182.
- Liu J, O'Connor WJ, Ahearne E, et al. (2013a) Electromechanical modelling for piezoelectric flextensional actuators. Smart materials and structures 23(2): 025005.
- Liu X, Vlajic N, Long X, et al. (2013b) Nonlinear motions of a flexible rotor with a drill bit: stick-slip and delay effects. *Nonlinear Dynamics* 72(1): 61–77.
- Liu X, Vlajic N, Long X, et al. (2014) Coupled axial-torsional dynamics in rotary drilling with state-dependent delay: stability and control. *Nonlinear Dynamics* 78(3): 1891–1906.
- Long X, Zheng P and Ren S (2017) Active delayed control of turning and milling dynamics. *Journal of Computational and Nonlinear Dynamics* 12(5): 051022.

- Monnin J, Kuster F and Wegener K (2014) Optimal control for chatter mitigation in milling—Part 2: experimental validation. *Control Engineering Practice* 24: 167–175.
- Nam S, Hayasaka T, Jung H, et al. (2020) Proposal of novel chatter stability indices of spindle speed variation based on its chatter growth characteristics. *Precision Engineering* 62: 121–133.
- Quintana G and Ciurana J (2011) Chatter in machining processes: a review. *International Journal of Machine Tools and Man-ufacture* 51(5): 363–376.
- Sallese L, Innocenti G, Grossi N, et al. (2017) Mitigation of chatter instabilities in milling using an active fixture with a novel control strategy. *The International Journal of Advanced Manufacturing Technology* 89(9): 2771–2787.
- Seguy S, Insperger T, Arnaud L, et al. (2010) On the stability of high-speed milling with spindle speed variation. The International Journal of Advanced Manufacturing Technology 48(9): 883–895.
- Seguy S, Insperger T, Arnaud L, et al. (2011) Suppression of period doubling chatter in high-speed milling by spindle speed variation. *Machining Science and Technology* 15(2): 153–171.
- Sheng X and Zhang X (2018) Fuzzy adaptive hybrid impedance control for mirror milling system. *Mechatronics* 53: 20–27.
- Tu G, Dong X, Chen S, et al. (2020) Iterative nonlinear chirp mode decomposition: a Hilbert-Huang transform-like method in capturing intra-wave modulations of nonlinear responses. *Journal of Sound and Vibration* 485: 115571–115571.
- Tu G, Dong X, Qian C, et al. (2021) Intra-wave modulations in milling processes. *International Journal of Machine Tools and Manufacture* 163: 103705.
- Wang X, Li Z, Bi Q, et al. (2019) An accelerated convergence approach for real-time deformation compensation in large thin-walled parts machining. *International Journal of Machine Tools and Manufacture* 142: 98–106.
- Yamato S, Ito T, Matsuzaki H, et al. (2018) Programmable optimal design of sinusoidal spindle speed variation for regenerative chatter suppression. *Procedia Manufacturing* 18: 152–160.
- Yamato S, Ito T, Matsuzaki H, et al. (2020) Self-acting optimal design of spindle speed variation for regenerative chatter suppression based on novel analysis of internal process energy behavior. *International Journal of Machine Tools and Manufacture* 159: 103639–103639.
- Yilmaz A, Al-Regib E and Ni J (2002) Machine tool chatter suppression by multi-level random spindle speed variation. *Journal* of Manufacturing Science and Engineering 124(2): 208–216.
- Zhang X, Wang C, Liu J, et al. (2019) Robust active control based milling chatter suppression with perturbation model via piezoelectric stack actuators. *Mechanical Systems and Signal Processing* 120: 808–835.
- Zhang Y and Sims ND (2005) Milling workpiece chatter avoidance using piezoelectric active damping: a feasibility study. Smart materials and structures 14(6): N65–N70.
- Zhao B, Cheng C, Tu G, et al. (2021) An interpretable denoising layer for neural networks based on reproducing kernel Hilbert space and its application in machine fault diagnosis. *Chinese Journal of Mechanical Engineering* 34(1): 44.
- Zhu L and Liu C (2020) Recent progress of chatter prediction, detection and suppression in milling. *Mechanical Systems and Signal Processing* 143: 106840.